DOI: 10.65731/ama/2026-0029

CONTINUOUS MODEL FOR VIBRATIONS OF THIN-WALLED BOX BEAMS FILLED WITH POLYMER CONCRETE

Beata NIESTEROWICZ*, Stefan BERCZYŃSKI*, Paweł DUNAJ*

*Department of Mechatronics, Faculty of Mechanical Engineering and Mechatronics,
West Pomeranian University of Technology in Szczecin, 17 Piastów Avenue, 70-310 Szczecin, Poland

beata.niesterowicz@zut.edu.pl, stefan.berczynski@zut.edu.pl, pawel.dunaj@zut.edu.pl

received 08 October 2025, revised 6 March 2026, accepted 12 March 2026

Abstract: This study presents a continuous analytical model for the dynamic analysis of thin-walled steel box beams filled with polymer concrete. The model incorporates transverse, longitudinal, and torsional vibrations, includes damping effects, and enables the calculation of frequency response functions. Its formulation is based on a coupled system of partial differential equations derived from Timoshenko beam theory and de Saint Venant's torsion model, providing a closed-form solution for modal parameters and vibrational response. Experimental validation performed on a steel-polymer concrete beam showed close agreement between predicted and measured natural frequencies, mode shapes, and frequency response functions. Additional comparisons with one-dimensional, three-dimensional finite element models as well as rigid finite element models from the literature confirmed that the proposed approach can serve as an attractive alternative to other computational methods. The model offers a favorable balance between accuracy and simplicity, making it well suited for preliminary design and vibration analysis of steel-polymer composite structures.

Key words: steel-concrete beam, thin-walled box beam, polymer concrete, Timoshenko beam theory, modal analysis, frequency response function

1. INTRODUCTION

Steel-concrete composite beams are widely used structural elements in mechanical and structural systems, where time-varying loads often induce vibrations [1] that affect performance [2] or safety [3]. Accurate prediction of their dynamic behavior has driven the development of various analytical and numerical modeling technique which offers complementary approaches for dynamic analysis of steel-concrete composite beams [4].

Analytical beam models remain popular due to their simplicity and the availability of closed-form or simplified numerical solutions. The classical formulation introduced by Euler and Bernoulli [5] assumes perfect bonding and neglects shear deformation and rotary inertia, leading to overestimated stiffness and natural frequencies, especially in short-span or thick composite beams. Timoshenko's refinement [6] addresses these limitations by incorporating shear flexibility and rotary inertia, providing more accurate frequency predictions for stocky members while maintaining a relatively simple mathematical form. More advanced approaches, such as Reddy's higher-order theory [7], relax the rigid cross-section assumption by introducing a cubic in-thickness displacement field, allowing cross-sectional warping and a more realistic shear stress distribution. This increased fidelity, however, comes at the cost of more complex governing equations that often lack closed-form solutions and require numerical techniques for implementation [8].

One example of steel-concrete composite beams analyzed using analytical models are beams consisting of a steel section with a reinforced concrete slab resting on it, as presented in the work of Berczyński and Wróblewski [9]. Authors investigated the free vibrations of steel-concrete composite beams consisting of a rolled IPE 140 steel beam connected to a reinforced concrete slab via steel stud connectors. Three analytical models were developed: two based on Euler beam theory, which included partial shear connection effects but assumed rigid cross-sections and neglected shear deformation and rotary inertia, and one based on Timoshenko beam theory. The latter accounted for shear flexibility and rotary inertia of the composite cross-section, leading to much closer agreement with experimental natural frequencies, particularly for higher vibration modes. The study demonstrated that including shear and rotational effects significantly improves dynamic modeling accuracy. These studies were later continued [10], where three composite beams with different connection stiffness were tested experimentally, and the Timoshenko model was complemented by a discrete rigid finite element model, both of which were successfully validated against modal test data and used to identify connection stiffness parameters.

Other researchers have extended analytical modeling to damage detection. Dilena and Morassi [11] proposed an analytical method for damage detection in steel-concrete composite beams based on vibration measurements. The authors developed an Euler-Bernoulli beam model incorporating a shear-type connection to represent partial interaction between steel and concrete, enabling the prediction of natural frequencies and mode shapes for both undamaged beams and those with partially degraded shear connectors. The model was experimentally validated through dynamic tests on specimens in both undamaged condition and with varying levels of connector damage, showing good agreement with the measured natural frequencies and mode shapes, including for intermediate damage states. To enhance modeling accuracy, the authors also

derived a refined version of the model based on Timoshenko beam theory. The method successfully identified the location and severity of damage through frequency shifts, although its sensitivity decreased for low damage levels.

Continuous analytical models provide an efficient means for predicting the global dynamic behavior of steel–concrete composite beams, offering fast evaluation of natural frequencies and mode shapes. Although well-suited for simplified geometries and boundary conditions, these models rely on idealized assumptions that limit their ability to accurately capture local phenomena such as interface slip, material discontinuities, and cross-sectional warping.

In parallel with analytical beam theories, numerical modeling techniques based on the finite element method [12] and its derivatives, including reduced-order models [13] and rigid finite element formulations [14], have become standard tools for analyzing steel-concrete composite beams. These methods, particularly the finite element method, enable detailed representation of complex geometries, material interfaces, and connection conditions, making them particularly suitable for layered or infilled structures.

Shen et al. [15] proposed a component-wise analytical approach based on the Carrera unified formulation [16] to study free vibration and stress analysis of steel–concrete composite beams. The method discretized the beam cross-section using Lagrange polynomials of different orders and allowed each material component to be modeled separately while automatically enforcing interfacial continuity. Closed-form Navier-type solutions were derived for simply supported beams and validated on I- and box-section steel-concrete composite beams. The results showed that the Carrera unified formulation component-wise approach can achieve three-dimensional accuracy in natural frequencies, mode shapes, and stress fields with significantly fewer degrees of freedom compared with full 3D finite element models. The main limitations include the assumption of perfect bonding between steel and concrete, linear elastic material behavior, and the focus on simple boundary conditions.

Henriques et al. [17] proposed a Generalized Beam Theory (GBT)-based finite element model for the dynamic analysis of steel-concrete composite beams [18], incorporating concrete cracking and cross-section deformation effects, including shear lag. The approach involves a two-step procedure: an incremental static analysis to account for non-linear behavior and to obtain the tangent stiffness matrix, followed by an eigenvalue analysis to compute natural frequencies and vibration mode shapes. The method makes use of GBT modal decomposition to represent structural deformation through a set of predefined cross-section modes, enabling reduced-order modeling with lower computational cost. The model was applied to simply supported beams subjected to uniform and eccentric loading, and the results were compared with those obtained from shell finite element models. Good agreement was observed in terms of natural frequencies and mode shapes, with significant reduction in the number of degrees of freedom. The method was also able to capture the influence of cracking on modal behavior. Limitations include simplified assumptions regarding concrete material behavior and the treatment of shear connection.

Assem et al. [19] proposed a refined quasi-3D beam theory combined with the differential quadrature finite element method to analyze free vibration of steel box-section beams infilled with porous polymer concrete cores. The study introduced different porosity distributions (uniform and two non-uniform patterns) and investigated their effects on natural frequencies under various boundary conditions and slenderness ratios. The model demonstrated high accuracy compared with experimental data and highlighted that strategically non-uniform porosity can maintain stiffness while reducing mass. However, the analysis assumed ideal material behavior and lacked experimental validation of porosity-specific configurations. In a subsequent study, the authors extended the proposed quasi-3D DQFEM framework to investigate the influence of crack presence and location on the dynamic behavior of composite steel–polymer concrete box-section beams [20].

The rigid finite element method [21] provides a reduced-order modeling approach for the dynamic analysis of steel-concrete composite beams. In this formulation, the structure is discretized into rigid segments interconnected by translational and rotational springs, efficiently capturing deformability while significantly reducing the number of degrees of freedom compared to conventional finite element models.

Abramowicz et al. [22] developed a three-dimensional rigid finite element model for steel-concrete composite beams, enabling analysis of flexural, torsional and distortional vibration modes that cannot be captured by conventional two-dimensional approaches. The model separately represents the concrete slab and steel I-section, linked by spring-damping elements to realistically reproduce connector dynamic properties. Dynamic tests were performed on two beams with different connector spacings, and model parameters (e.g., connector stiffness and equivalent longitudinal modulus of the concrete slab) were identified using natural frequencies and mode shapes from impulse response experiments. The validated model showed good agreement with experimental results and was applied to simulate connector damage, demonstrating the feasibility of vibration-based damage detection for composite structures

Dunaj et al. [23] applied the rigid finite element method to model the dynamic behavior of a steel beam filled with polymer concrete, aiming to provide a low-dimensional yet accurate alternative to conventional finite element models. The proposed approach aggregated the mass and stiffness of steel and polymer concrete into discrete rigid elements connected by spring-damping elements, enabling efficient calculation of natural frequencies, mode shapes, and frequency response functions. Modal testing confirmed good agreement in terms of mode shapes and natural frequencies, while the model significantly reduced computational complexity compared to full 3D FEM simulations. Reported limitations include reduced accuracy in predicting non-resonant frequency response.

The reviewed literature indicates that continuous analytical models and finite element models offer complementary strengths and limitations in the dynamic analysis of steel-concrete composite beams. Continuous models provide closed-form expressions for natural frequencies and mode shapes with minimal computational effort. They are well suited for parametric studies, damage detection, and theoretical investigations but rely on simplifying assumptions such as perfect bonding, uniform cross-sections, and linear material behavior, which may limit their applicability to complex or layered structures. Conventional finite element models, in contrast, offer high accuracy and flexibility, allowing detailed representation of material interfaces, geometry, and boundary conditions. However, this comes with increased computational cost and greater modeling complexity. The rigid finite element method provides a reduced-order alternative by discretizing the structure into rigid segments connected by translational and rotational springs [24]. This approach enables an efficient representation of deformability, particularly useful for capturing partial shear interaction and interface slip, while significantly reducing the number of degrees of freedom. Its limitations include reduced accuracy in modeling non-resonant dynamic behavior and the use of simplified, often isotropic, material properties.

DOI: 10.65731/ama/2026-0029

Although considerable progress has been made in modeling the dynamic behavior of steel-concrete composite beams, certain aspects remain the subject of ongoing development. In particular, comprehensive continuous analytical models that account for all fundamental vibration modes – transverse, longitudinal, and torsional – and enable the evaluation of amplitude-frequency response characteristics are still limited. To contribute to this area, the present study proposes a continuous analytical model for thin-walled box-section beams filled with polymer concrete, which captures transverse, longitudinal, and torsional vibrations. The equations of motion are derived using Hamilton's principle, ensuring a consistent formulation grounded in energy methods. By incorporating damping, the model enables direct evaluation of frequency response functions, providing a more complete dynamic characterization. The homogenized formulation adopted in this study enables efficient evaluation of global dynamic characteristics while maintaining sufficient accuracy, which makes it particularly suitable for parametric analyses and iterative computational procedures, where component-wise models would lead to significantly higher computational cost. The proposed model has been experimentally verified and validated using reference data from the literature, confirming its suitability for analyzing the vibration performance of steel-polymer concrete composite beams.

The paper is organized as follows: Section 2 introduces the research object, a steel-polymer concrete beam, and its static and dynamic experimental testing. Section 3 presents the modeling methodology, including key assumptions and formulations. Section 4 reports the results, verifying the proposed modeling approach and comparing its accuracy with alternative methods from the literature. Section 5 discusses the findings, and Section 6 concludes with key insights, limitations, and directions for future work.

2. MATERIALS AND METHODS

2.1. Research object

The research object is a steel-polymer concrete beam designed to combine the stiffness of steel with the vibration-damping capability of polymer concrete. The analyzed beam used a square steel profile with a cross-section of 70 × 70 mm, a wall thickness of 3 mm and a length of 1000 mm. The profile was filled with polymer concrete and compacted to ensure complete filling. The polymer concrete composition, based on previous studies [25,26], consisted of epoxy resin and mineral aggregates of various grain sizes. The aggregates were divided into fractions according to grain size: ash, a fine fraction (mainly sand, 0.25-2 mm), a medium fraction (2-10 mm), and a coarse fraction (8-16 mm, primarily irregularly shaped gravel). The mass percentages of individual fractions are presented in Tab. 1. The structure of a steel-polymer concrete beam is shown in Fig. 1.

Tab. 1. Composition of the applied polymer concrete filling

Component	Epoxy resin	Ash	Fine fraction (0.25-2 mm)	Medium fraction (2-10 mm)	Coarse fraction (8-16 mm)
Weight percent	15 %	1 %	19 %	15 %	50 %

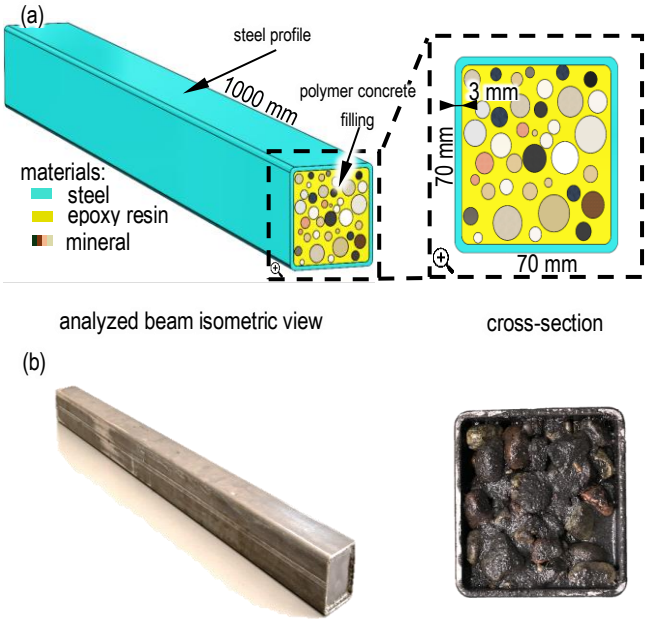

Fig. 1. Structure of the steel-polymer concrete beam, schematic view (a), and real structure (b)

2.2. Static tests

Static compression tests were performed to determine the material constants required for modelling. Cuboidal samples of steel (50 × 50 × 110 mm) and polymer concrete (45 × 45 × 110 mm) were tested on an Instron 8850 machine (Instron, Norwood, MA, USA) under controlled laboratory conditions (23 °C, 50 % relative humidity). The setup included a class 0.5 load cell (250 kN capacity) and a class 0.2 Instron 2620-603 tactile extensometer with measuring ranges of 25 mm and 12.5 mm (±1 mm). Samples were conditioned for 72 h prior to testing. Material properties with associated standard uncertainties and the loss factor, determined from dynamic tests using the half-power method, are presented in Tab. 2.

Tab. 2. Material properties of steel and polymer concrete determined based on the experimental study

Property	Steel	Polymer concrete
Modulus of elasticity	$E_s = 210 \pm 5$ GPa	$E_p = 17.2 \pm 0.2$ GPa
Poisson's ratio	$\upsilon_s = 0.28 \pm 0.03$	$\upsilon_p = 0.20 \pm 0.05$
Density	$\rho_s = 7812 \pm 35$ kg/m³	$\rho_s = 2200$ kg/m³ ± 26 kg/m³

2.3. Dynamic tests

Experimental modal analysis was performed to determine the modal parameters of the manufactured beams, both empty and filled with polymer concrete. Free boundary conditions were approximated by suspending the beams on steel cables, with suspension points (100 mm from each end) and cable stiffness chosen to reproduce natural vibration modes within the target frequency range.

The measurement setup was designed to capture at least the first five deformable vibration modes (20-2600 Hz). Impulse

excitation was applied using a PCB 086C01 (PCB Piezotronics, Depew, NY, USA) modal hammer with a polymer tip, providing sufficient bandwidth. To capture transverse, torsional, and longitudinal responses, excitation was applied in three perpendicular directions (+X, −Z, −Y); torsional modes were additionally identified by off-axis excitation in the −Z direction. Excitation points were selected to avoid nodal regions, located approximately 420 mm from the beam end for Z and Y excitations, and at the closed end for X-direction excitation.

Responses were measured using eight ICP PCB 356A01 (PCB Piezotronics, Depew, NY, USA) piezoelectric accelerometers mounted simultaneously sing wax as the adhesive. Three-axis measurements were taken at eight points in each of seven successive sections, resulting in 56 measurement locations. The sensors were repositioned sequentially to ensure complete spatial coverage. The parameters of the impact testing measurement system components are presented in Tab. 3.

Tab. 3. Experimental equipment parameters

Parameter	Value
PCB 086C01 modal hammer (PCB Piezotronics, Depew, NY, USA)	
sensitivity (±15 %)	10.23 mV/N
measurement range	±444 N pk
hammer mass	0.10 kg
head mass	0.03 kg
tip	polymer
PCB 356A01 three-axis piezoelectric accelerometer (PCB Piezotronics, Depew, NY, USA)	
sensitivity: (±20 %)	5 mV/g
measurement range	±1000 g pk
weight (without cable)	0.001 kg
frequency range	2-8000 Hz

Measurement signals were processed using a Scadas Mobile Vibco system with Simcenter LMS Testlab software (Siemens AG, Munich, Germany). Sampling was performed at 8,192 Hz with a frequency resolution of 0.25 Hz. Each transfer function was estimated from 7 repeated excitations using the H1 estimator, and signals were recorded for 4 s, allowing the response to decay without windowing.

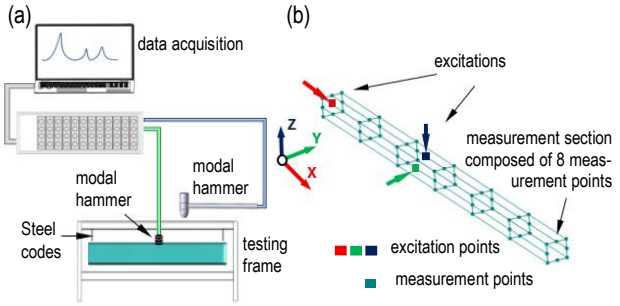

Fig. 2. Test stand for conducting impact tests: schematic view (a) excitation and measurement points arrangement (b)

3. CONTINUOUS MODEL OF BEAM VIBRATIONS

3.1. Model assumptions

Based on experimental observations, several simplifications were adopted to develop the mathematical model of the beam. Despite the heterogeneous structure of polymer concrete, its dynamic behavior was represented by a linear elastic material model. This assumption was supported by experimental results demonstrating compliance with Maxwell's reciprocity principle, linear stiffness characteristics and symmetric mode shapes obtained from impulse testing, as detailed in [27,28]. Perfect contact between the steel profile and the polymer concrete filling was assumed along the entire internal surface, with adhesion preventing tangential slip at the interface.

3.2. Longitudinal vibrations

The longitudinal vibration model was derived using Hamilton's principle, assuming that the deformation of the cross-section in the transverse directions (v and w) is negligible. Accordingly, the displacement components (Fig. 3) in each direction can be expressed as:

$$u_s = u_p = u_c(x,t) \quad v_s = v_p = 0 \quad w_s = w_p = 0 \tag{1}$$

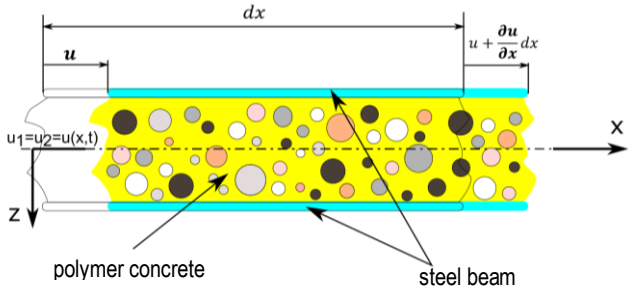

Fig. 3. Displacement definitions for the longitudinal vibration model of a square-section beam

Using the total equivalent coefficients, the potential π and kinetic T energies of the composite beam are expressed as:

$$\pi = \frac{1}{2}\iiint_{V_c}(\sigma_{xx}\varepsilon_{xx})dV_c = \frac{1}{2}\int_0^l \left[(EA)_c\left(\frac{\partial u_c}{\partial x}\right)^2\right]dx, \tag{1}$$

$$T = \frac{1}{2}\int_0^l \left[(\rho A)_c\left(\frac{\partial u_c}{\partial t}\right)^2\right]dx \tag{3}$$

From equations (2) and (3), the equivalent coefficients for a composite beam can be determined as the sum of the stiffness and mass coefficients of its individual components sharing a common neutral axis. The longitudinal stiffness $(EA)_c$ and mass per unit length $(\rho A)_c$ for composite beam depend on steel and polymer concrete properties and are given by:

$$(EA)_c = E_s A_s + E_p A_p, \tag{4}$$

$$(\rho A)_c = \rho_s A_s + \rho_p A_p \tag{5}$$

Applying Hamilton's principle, the equation of motion of the beam along the x-axis is obtained as:

DOI: 10.65731/ama/2026-0029

$$(EA)_c \frac{\partial^2 u_c}{\partial x^2} = (\rho A)_c \frac{\partial^2 u_c}{\partial t^2} \tag{6}$$

Assuming a separable solution, the equation can be written as:

$$u_c(x,t) = U(x)Q(t) \tag{7}$$

where $U(x)$ is the axial displacement amplitude and $Q(t)$ describes the harmonic motion. Substituting into equation (7) yields:

$$\frac{\partial^2 U(x)}{\partial x^2} + p_w \omega^2 \, U(x) = 0 \tag{8}$$

where:

$$p_w = \frac{(EA)_c}{(\rho A)_c}. \tag{9}$$

The function $U(x)$ representing the longitudinal vibration modes, can be written as:

$$U(x) = C_1 cos\frac{\omega x}{p_w} + \mathrm{C}_2 \sin\frac{\omega x}{p_w} \tag{10}$$

where the integration constants C_1 and C_2 are determined from the boundary conditions. For a free beam, zero axial force at both ends gives the boundary conditions:

$$(EA)_c \frac{\partial u_c}{\partial x}(x,t) = 0, \; x = 0, L. \tag{11}$$

Substituting the boundary conditions into equation (10) yields the frequency equation, whose solution gives the natural frequencies:

$$\sin\frac{\omega L}{p_w} = 0 \tag{12}$$

for which the solutions take the form

$$\omega_r = \frac{r\pi p_w}{L} \tag{13}$$

where $r = 0, 1, 2, 3, \ldots, \infty$ denotes the mode number.

Assuming the orthonormality condition:

$$\int_{x=0}^{x=L} \widetilde{U}_r(x)(\rho A)_c \widetilde{U}_r(x)dx = 1 \tag{14}$$

The normalized rigid and flexible longitudinal mode shapes were obtained as:

$$\widetilde{U}_0(x) = \sqrt{\frac{1}{(\rho A)_c L}}, \; r = 0, \tag{15}$$

$$\widetilde{U}_r(x) = \sqrt{\frac{2}{(\rho A)_c L}} cos\frac{r\pi p_w x}{L}, \; r = 1, 2, 3, \ldots, \infty. \tag{16}$$

3.3. Torsional vibrations

Because the analyzed beam has a cross-section symmetric about both principal axes, torsion can be treated as independent of other vibration modes. However, due to the square cross-section, distortion occurs during twisting. To account for this effect when determining torsional natural frequencies, the de Saint Venant model was applied, including a correction for displacement caused by cross-section warping. Introducing the warpage function $\Psi^w(y,z)$ allows representation of the axial displacement associated with this distortion. In practice, this requires zero normal shear stress at every point of the end sections. The resulting displacements (Fig. 4) in all three directions are expressed as:

$$u_s = u_p = \Psi^w(y,z)\frac{\partial \theta_c}{\partial x}, v_s = v_p = -z\theta_c(x,t), \; w_s = w_p = y\theta_c(x,t) \tag{17}$$

where $\frac{\partial \theta_c}{\partial x}$ is the torsion rate along the beam axis, assumed constant.

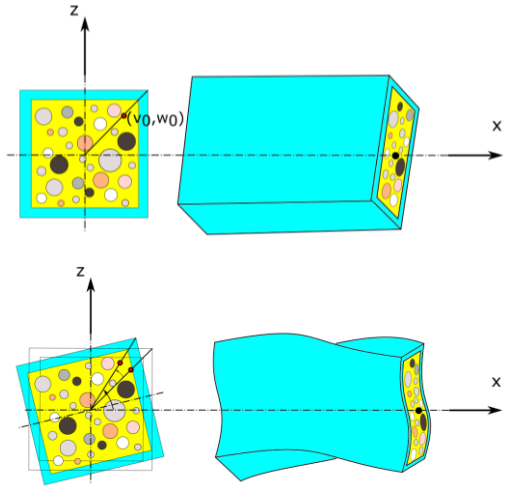

Fig. 4. Displacement definitions in the de Saint Venant torsion model for a square-section beam

The potential and kinetic energies of the composite beam are given by:

$$\pi = \frac{1}{2}\iiint_{V_c} (\sigma_{xy}\gamma_{xy} + \sigma_{xz}\gamma_{xz})dV_c = \\ = \frac{1}{2}\int_0^l \iint_{A_c} G_c \left[\left(\frac{\partial \Psi^w}{\partial y} - z\right)^2 + \left(\frac{\partial \Psi^w}{\partial z} + y\right)^2\right] dA_c \left(\frac{\partial \theta_c}{\partial x}\right)^2 dx = \frac{1}{2}\int_0^l (GJ)_c \left(\frac{\partial \theta_c}{\partial x}\right)^2 dx, \tag{18}$$

$$T = \frac{1}{2}\iiint_{V_c} \left[\rho_c \left[\left(\frac{\partial u_c}{\partial t}\right)^2 + \left(\frac{\partial v_c}{\partial t}\right)^2 + \left(\frac{\partial w_c}{\partial t}\right)^2\right]\right] dV_c = \\ = \frac{1}{2}\int_0^l \iint_{A_c} \rho_c (\Psi^w)^2 \left(\frac{\partial^2 \theta_c}{\partial t \partial x}\right)^2 dA_c + (\rho I^p)_c \left(\frac{\partial \theta_c}{\partial t}\right)^2 dx. \tag{19}$$

where J is the torsion constant, dependent on the beam cross-section [29]. For a solid square beam, $J_p = 0.1406{h_1}^4$ and for a thin-walled square section, $J_s = 0.0625(h_1 - h_2)^4$. For beams sharing a common neutral axis, the equivalent torsional stiffness and mass polar moment of inertia are:

$$(GJ)_c = (GJ)_s + (GJ)_p, \tag{20}$$

$$(\rho I^p)_c = (\rho I^p)_s + (\rho I^p)_p \tag{21}$$

where I^p is the polar moment of inertia, defined as $I^p = \iint_A (x^2 + z^2)dA$. Applying Hamilton's principle, the equation of motion for torsional vibrations is:

$$(\rho \mathrm{I}^{\mathrm{p}})_c \frac{\partial^2 \theta_c(x,t)}{\partial t^2} = (GJ)_c \frac{\partial^2 \theta_c(x,t)}{\partial x^2}. \tag{22}$$

Assuming a separable solution, the equation can be written as:

$$\theta_c(x,t) = \Theta(x)Q(t), \tag{23}$$

where $\Theta(x)$ is the torsional displacement amplitude and $Q(t)$ represents the harmonic motion. Substituting into equation (22) gives:

$$\frac{\partial^2\Theta(x)}{\partial x^2} + p_s\omega^2\,\Theta(x) = 0, \tag{24}$$

where:

$$p_s = \frac{(GJ)_c}{(\rho I^p)_c}. \tag{25}$$

The function $\Theta(x)$, representing the torsional vibration modes, can be written as:

$$\Theta(x) = C_1\cos\frac{\omega x}{p_s} + C_2\sin\frac{\omega x}{p_s}. \tag{26}$$

where the integration constants C_1 and C_2 are determined from the boundary conditions. For a free beam, zero torque at both ends gives the boundary conditions:

$$(GJ)_c\frac{\partial\theta_c}{\partial x}(x,t) = 0,\ x = 0, L. \tag{27}$$

Substituting the boundary conditions into equation (26) yields the frequency equation, whose solution gives the natural frequencies:

$$\sin\frac{\omega L}{p_s} = 0, \tag{28}$$

for which the solutions take the form

$$\omega_r = \frac{r\pi p_s}{L},\ r = 0,1,2,3,\dots,\infty. \tag{29}$$

Assuming the orthonormality condition:

$$\int_{x=0}^{x=L}\tilde{\Theta}_r(x)(\rho I)_c\tilde{\Theta}_r(x)dx = 1. \tag{30}$$

The normalized rigid and flexible torsional mode shapes were obtained as:

$$\tilde{\Theta}_0(x) = \sqrt{\frac{1}{(\rho I)_c L}},\ r = 0, \tag{31}$$

$$\tilde{\Theta}_r(x) = \sqrt{\frac{2}{(\rho I)_c L}}\cos\frac{r\pi p_s x}{L},\qquad r = 1,2,3,\dots,\infty. \tag{32}$$

3.4. Transverse vibrations

To derive the equations of motion using Timoshenko's theory, the displacement variables were defined as:

$$u_s = u_p = -z\left(\frac{\partial w_c}{\partial x} - \frac{\partial(w^s)_c}{\partial x}\right) = -z\phi_c,\qquad v_s = v_p = 0,$$
$$w_s = w_p = w_c(x,t) \tag{33}$$

where ϕ is the cross-section rotation, w is the bending displacement, and w^s is the shear displacement, as shown in Fig. 5.

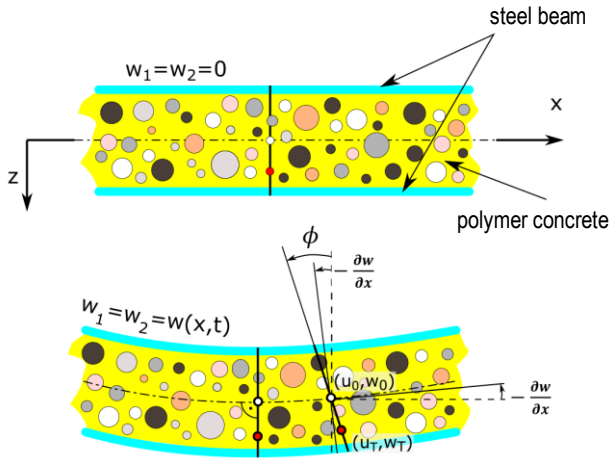

Fig. 5. Longitudinal cross-section of a polymer-concrete beam under bending, showing undeformed and deformed shapes according to Timoshenko's theory

The shear coefficient κ accounts for the non-uniform shear strain distribution and cross-section distortion [30]. Applying Hamilton's principle with Timoshenko's theory, the coefficients of the composite beam equations were derived. The potential and kinetic energies of the composite beam are given by:

$$\pi = \frac{1}{2}\iiint_{V_c}(\sigma_{xx}\varepsilon_{xx} + \sigma_{zx}\gamma_{zx})dV_c = \frac{1}{2}\int_0^l\left[E_sI_s\left(\frac{\partial\phi_c}{\partial x}\right)^2 + \kappa_sA_sG_s\left(\frac{\partial w_c}{\partial x} - \phi_c\right)^2 + E_pI_p\left(\frac{\partial\phi_c}{\partial x}\right)^2 + \kappa_pA_pG_p\left(\frac{\partial w_c}{\partial x} - \phi_c\right)^2\right]dx, \tag{34}$$

$$T = \frac{1}{2}\int_0^l\left[\rho_sA_s\left(\frac{\partial w_c}{\partial t}\right)^2 + \rho_sI_s\left(\frac{\partial\phi_c}{\partial t}\right)^2 + \rho_pA_p\left(\frac{\partial w_c}{\partial t}\right)^2 + \rho_pI_p\left(\frac{\partial\phi_c}{\partial t}\right)^2\right]dx \tag{35}$$

For free vibrations, external forces are absent; hence, the work of external forces is zero.

$$\delta\int_{t_1}^{t_2}(\pi - T)dt = 0, \tag{36}$$

$$\delta_c\int_{t_1}^{t_2}\int_0^l\left(\left[\left(E_sI_s + E_pI_p\right)\left(\frac{\partial\phi_c}{\partial x}\right) + \kappa_c\left(A_sG_s + A_pG_p\right)\left(\frac{\partial w_c}{\partial x} - \phi_c\right)\left(\frac{\partial w_c}{\partial x}\right) - \kappa_c\left(A_sG_s + A_pG_p\right)\left(\frac{\partial w_c}{\partial x} - \phi_c\right)\phi_c\right] - \left[\left(\rho_sA_s + \rho_pA_p\right)\frac{\partial w_c}{\partial t}\left(\frac{\partial w_c}{\partial t}\right) + \left(\rho_sI_s + \rho_pI_p\right)\frac{\partial\phi_c}{\partial t}\left(\frac{\partial\phi_c}{\partial t}\right)\right]\right)dx\,dt = 0. \tag{37}$$

From equations (36) and (37), the equivalent coefficients for composite beams can be determined from the flexural stiffness $(EI)_c$, shear stiffness $(AG)_c$ and mass moment of inertia $(\rho I)_c$ of individual components sharing a common neutral axis.

$$(EI)_c = E_sI_s + E_pI_p. \tag{38}$$

$$(AG)_c = A_sG_s + A_pG_p. \tag{39}$$

$$(\rho I)_c = \rho_sI_s + \rho_pI_p. \tag{40}$$

DOI: 10.65731/ama/2026-0029

Using integration by parts and grouping terms, the equation for a uniform beam can be expressed as a system of two differential equations in terms of the displacement w_c and rotation angle ϕ_c:

$$-\kappa_c(AG)_c\frac{\partial^2 w_c}{\partial x^2}+\kappa_c(AG)_c\frac{\partial \phi_c}{\partial x}+(\rho A)_c\frac{\partial^2 w_c}{\partial t^2}=0, \tag{41}$$

$$-(EI)_c\frac{\partial^2 \phi_c}{\partial x^2}-\kappa_c(AG)_c\frac{\partial w_c}{\partial x}+\kappa_c(AG)_c\phi_c+(\rho I)_c\frac{\partial^2 \phi_c}{\partial t^2}=0. \tag{42}$$

The general solution of these equations for natural vibrations can be written as:

$$w_c(x,t)=W(x)Q(t),\quad \phi_c(x,t)=\Psi(x)Q(t), \tag{43}$$

where $W(x)$ and $\Psi(x)$ are the amplitudes of the displacement $w_c(x,t)$ and rotation angle $\phi_c(x,t)$, respectively, and $Q(t)$ represents the harmonic motion. After substitution and simplification, equations (41) and (42) become:

$$\frac{\partial^4 W(x)}{\partial x^4}+P\frac{\partial^2 W(x)}{\partial x^2}+SW(x)=0, \tag{44}$$

$$\frac{\partial^4 \Psi(x)}{\partial x^4}+P\frac{\partial^2 \Psi(x)}{\partial x^2}+S\Psi(x)=0, \tag{45}$$

where:

$$P=p^4(q^2+s^2), \tag{46}$$

$$S=p^4(p^4s^2q^2), \tag{47}$$

$$p^4=\frac{L^4(\rho A)_c\omega^2}{(EI)_c},\ q^2=\frac{(\rho I)_c}{(\rho A)_cL^2},\ s^2=\frac{(EI)_c}{\kappa_c(AG)_cL^2}. \tag{48}$$

After variable separation, the transverse vibration mode functions for $\omega=\omega_r$ can be expressed as:

$$W_r(x)=A_r\left[C_1\sin\frac{\lambda_1 x}{L}+C_2\cos\frac{\lambda_1 x}{L}+C_3\sinh\frac{\lambda_2 x}{L}+C_4\cosh\frac{\lambda_2 x}{L}\right], \tag{49}$$

$$\Psi_r(x)=A_r\left[D_2\cos\frac{\lambda_1 x}{L}+D_1\sin\frac{\lambda_1 x}{L}+D_4\cosh\frac{\lambda_2 x}{L}+D_3\sinh\frac{\lambda_2 x}{L}\right], \tag{50}$$

where $r=1,2,3,\ldots,\infty$ denotes the mode number.

$$\lambda_1=\sqrt{\frac{H+\sqrt{H^2-4F}}{2}},\qquad \lambda_2=\sqrt{\frac{-H+\sqrt{H^2-4F}}{2}}. \tag{51}$$

The four integration constants C_m where $m=1,2,3,4$ for the translational displacement function $W_r(x)$ and C_m where $m=1,2,3,4$ for the rotational displacement function $\Psi_r(x)$ are mutually dependent. Their relationship is obtained by substituting equations (43) into (42) and inserting (49) and (50) into the result, yielding:

$$D_1=-\frac{p^4s^2-\lambda_1^2}{L\lambda_1}C_2,\quad D_2=\frac{p^4s^2-\lambda_1^2}{L\lambda_1}C_1, \tag{52}$$

$$D_3=\frac{p^4s^2+\lambda_2^2}{L\lambda_2}C_4,\quad D_4=\frac{p^4s^2+\lambda_2^2}{L\lambda_2}C_3.$$

The constant A_r in equations (49) and (50), as in the longitudinal and torsional cases, is obtained by normalizing the mode function with respect to the modal mass to satisfy the orthonormality condition. This condition is expressed as:

$$\int_{x=1}^{x=L}\{Y_r(x)\}^T[\mathbb{M}]\{Y_n(x)\}dx=\begin{cases}1, r=n\\0, r\neq n\end{cases}, \tag{53}$$

where the natural vibration mode vector and mass matrix are given by:

$$\{\mathrm{Y_r(x)}\}=\begin{Bmatrix}\mathrm{W_r(x)}\\ \Psi_\mathrm{r}(\mathrm{x})\end{Bmatrix}, \tag{54}$$

$$[\mathbb{M}]=\begin{bmatrix}(\rho\mathrm{A})_c & 0\\ 0 & (\rho\mathrm{I})_c\end{bmatrix}. \tag{55}$$

The integration coefficients C_m of the transverse vibration modes are determined from the boundary conditions. For a free beam, the zero shear force N and bending moment M for the Timoshenko model are expressed as:

$$(EI)_c\frac{\partial \phi_c}{\partial x}(x,t)=0,\qquad x=0, \tag{56}$$

$$\kappa_c(GA)_c\left(\frac{\partial w_c}{\partial x}(x,t)-\phi_c(x,t)\right)=0,\ x=0,L \tag{57}$$

Using all four boundary conditions and the relationship between the C_m and D_m coefficients, a 4 × 4 matrix $\mathbb{D}$ was obtained. The transverse natural frequencies are determined by solving:

$$\mathbb{D}(\omega)C=0, \tag{58}$$

To solve the system of equations (58), the determinant of matrix $\mathbb{D}$ was computed, and its zeros were used to obtain the transverse natural frequencies. The integration constants were determined numerically using matrix factorization, and the corresponding natural vibration modes were plotted for the identified frequencies. Following [31], the translational and rotational rigid forms, resulting from the beam's displacement and rotation relative to its centre of gravity, are expressed as:

$$W_0^{trans}(x)=\sqrt{\frac{1}{(\rho A)_cL}}, \tag{59}$$

$$\Psi_0^{rot}(x)=\sqrt{\frac{12}{(\rho A)_cL^3}}\left(x-\frac{L}{2}\right). \tag{60}$$

3.5. Damping

To determine the system response to excitation, damping was included in the model. A constant damping coefficient was assumed for the entire frequency range using a hysteretic model. Starting from the distributed internal viscous damping relationship [32] in Hamilton's principle and considering the Rayleigh dissipation function R [32], the translational and rotational motion equations with damping are given by:

$$(EI)_c(1+j\eta)W^{IV}+(\rho A)_c\omega^2W-(\rho I)_c\left(1+\frac{(EA)_c}{\kappa_c(AG)_c}\right)\omega^2W^{II}+\frac{(\rho A)_c(\rho I)_c}{\kappa_c(AG)_c(1+j\eta)}\omega^4W=0, \tag{61}$$

$$(EI)_c(1+j\eta)\Psi^{IV} + (\rho A)_c\omega^2\Psi - (\rho I)_c\left(1 + \frac{(EA)_c}{\kappa_c(AG)_c}\right)\omega^2\Psi^{II} + \frac{(\rho A)_c(\rho I)_c}{\kappa(AG)_c(1+j\eta)}\omega^4\Psi = 0. \quad (62)$$

To account for internal damping in the continuous model, the composite longitudinal and transverse stiffnesses were assumed as:

$$E_c^* = E_c(1+j\eta_c), \quad (63)$$

$$G_c^* = G_c(1+j\eta_c). \quad (64)$$

The general equation of motion for forced vibrations of a uniform cross-section beam with damping is written as:

$$(EI)_c(1+j\eta_c)\frac{\partial^4 w_c(x,t)}{\partial x^4} + (\rho A)_c\frac{\partial^2 w_c(x,t)}{\partial t^2} = f(x,t). \quad (65)$$

Forced vibration problems can be solved using the eigenfunction superposition method or a closed-form solution.

4. RESULTS

4.1. Steel-polymer concrete beam parameters

The analyzed beam features a square hollow steel section with an external cross-section of 70 × 70 mm, wall thickness of 3 mm, and total length of 1000 mm. The internal volume is completely filled with polymer concrete. The effective material and geometric parameters of the composite section were determined using classical homogenization rules and are listed in Tab. 4.

Tab. 4. Material and cross-sectional parameters used in the model

Parameter	Symbol	Value	Unit
Square hollow steel section			
Modulus of elasticity	E_s	$2.05\cdot10^{11}$	MPa
Poisson's ratio	υ_s	0.28	-
Density	ρ_s	$7.8\cdot10^{3}$	kg/m^3
Loss factor	η_s	$2.2\cdot10^{-3}$	-
Cross-sectional area	A_s	$8.04\cdot10^{-4}$	m^2
Second moment of area	I_s	$6.03\cdot10^{-7}$	m^4
Torsional constant	J_s	$1.02\cdot10^{-6}$	m^4
Polar moment of inertia	I_s^p	$1.21\cdot10^{-6}$	m^4
Polymer concrete infill section			
Modulus of elasticity	E_p	$1.72\cdot10^{10}$	MPa
Poisson's ratio	υ_p	0.2	-
Density	ρ_p	$2.2\cdot10^{3}$	kg/m^3
Loss factor	η_p	$1.52\cdot10^{-2}$	-
Cross-sectional area	A_p	$4.1e\cdot10^{-3}$	m^2
Second moment of area	I_p	$1.40\cdot10^{-6}$	m^4
Torsional constant	J_p	$2.36\cdot10^{-6}$	m^4
Polar moment of inertia	I_p^p	$2.80\cdot10^{-6}$	m^4

The shear coefficient κ_c was set to 5/6. Material damping was modeled using a structural damping model with a constant loss factor η. For the frequency response analysis, it was expressed in the modal domain as equivalent viscous damping in each vibrational mode, calibrated using experimental frequency response data. Using the test stand depicted in Fig. 2, the loss factor η of the composite steel-polymer concrete beam was determined through frequency response function measurements, applying the half-power method described in [23], which yielded a value of $\eta = 0.00480$.

4.2. Experimental verification of mode shapes and natural frequencies

To verify the predictive capability of the developed continuous model, a comparison was carried out between the calculated and experimentally measured natural frequencies. The analysis included transverse, torsional, and longitudinal modes to evaluate the model's ability to capture diverse types of vibrational behavior. The accuracy of the predictions is presented in Tab. 4, which summarizes the results for the test specimen described in Subsection 2.1 – a square steel beam with a 70 × 70 mm cross-section, 3 mm wall thickness, and a total length of 1000 mm. Tab. 5 includes relative error values δ with respect to the experimental results.

Tab. 5. Comparison of experimental and predicted natural frequencies for the 70 × 70 mm, 3 mm wall, 1000 mm long beam

Mode number	Mode type	Experiment, Hz	Developed model, Hz	Relative error δ, %
1.	1st trans.	340	342	0.6
2.	1st trans.	341	342	0.3
3.	2nd trans.	899	902	0.3
4.	2nd trans.	902	902	0
5.	1st tors.	1264	1246	1.4
6.	3rd trans.	1665	1672	0.4
7.	3rd trans.	1672	1672	0
8.	1st long.	2003	1959	2.2
9.	2nd tors.	2520	2491	1.2
10.	4th trans.	2571	2592	0.8
11.	4th trans.	2573	2592	0.7
			Average:	**0.7**

The comparison presented in Tab. 5 confirms full agreement of mode shapes, indicating that the developed model accurately captured the first eleven modes of the composite beam. The predicted natural frequencies match the experimental results with a mean relative error of 0.7 % and a maximum deviation of 2.2 %, observed for the first longitudinal mode (mode 8). Transverse modes, which dominate the dynamic response, were reproduced with high precision, with several modes (modes 4 and 7) showing zero error and others deviating by less than 0.6 %. Torsional modes were slightly underestimated, with relative errors below 1.5 %, while longitudinal behavior was less accurately captured. Overall, the results confirm the suitability of the continuous model for predicting global dynamic characteristics across multiple mode types.

Frequency response functions for both the experimental setup and the model were plotted. Excitation was applied at 7/12 of the beam length from one end, and responses were measured at 2/12 of the length. Fig. 6 presents the linear and logarithmic receptance functions of the analytical model compared with those of the tested beam.

As shown in Fig. 5, the measured and predicted receptance functions display very similar resonance peaks and frequency locations. The agreement in amplitude and curve shape indicates that the developed continuous model provides a reliable approximation of the dynamic response of the tested beam in both transverse directions.

DOI: 10.65731/ama/2026-0029

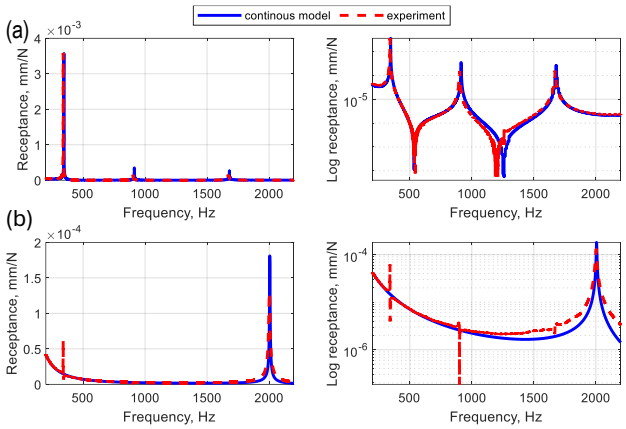

Fig. 6. Receptance functions of the 70 × 70 mm, 3 mm wall, 1000 mm beam from the developed model and experimental measurements in Z direction (a) and X direction (b)

4.3. Comparison with Other Modeling Approaches

To further evaluate the applicability of the proposed continuous model, its results were compared with those obtained using alternative modeling approaches and with data reported for beams of different dimensions. This comparison serves as an additional form of validation, assessing the model's ability to predict dynamic properties beyond the specific geometry tested experimentally. It also highlights the model's performance relative to other commonly used analytical and numerical methods. Tab. 6 presents a comparison between the developed continuous model and two finite element-based approaches: (i) a one-dimensional beam element model (based on a classical beam theory) and (ii) a full three-dimensional finite element model, both reported in [23]. Tab. 6 has been supplemented with relative error values referenced to the experimental results. The notation is as follows: δ denotes the relative error for the proposed continuous model, δ_{3D} for the three-dimensional finite element model, and δ_{1D} for the one-dimensional finite element model (based on Euler-Bernoulli theory).

The results in Tab. 6 highlight the differences in predictive accuracy between the continuous model and the two finite element approaches. The continuous model achieved a mean relative error of 2.4 %, closely matching the experimental frequencies and demonstrating consistent performance across both transverse and torsional modes. The full three-dimensional finite element model showed slightly better accuracy, with an average error of 1.9 %, reflecting its capacity to capture detailed geometric and material characteristics. In contrast, the one-dimensional beam element model exhibited the largest deviations, with an average error of 4.2 %, particularly underestimating torsional and higher-order transverse modes – a characteristic limitation due to its foundation in Euler–Bernoulli beam theory. These findings suggest that while 3D finite element models offer the highest fidelity, the continuous model provides a favorable balance between accuracy and computational efficiency, outperforming the conventional one-dimensional approach. However, to fully substantiate this observation, a direct comparison with a one-dimensional model based on Timoshenko beam theory would be necessary.

Tab. 6. Comparison of experimental and finite element models-predicted natural frequencies for the 50 × 50 mm, 2 mm wall, 1000 mm long beam

M. no	Mode type	Experiment, Hz	Developed model, Hz	δ, %	Finite element models			
					3D, Hz	δ_{3D}, %	1D, Hz	δ_{1D}, %
1.	1st trans.	247	245	0.8	248	0.4	243	1.6
2.	1st trans.	251	245	2.4	248	1.2	243	3.2
3.	2nd trans.	676	657	2.8	685	1.3	650	3.8
4.	2nd trans.	678	657	3.1	685	1	650	4.1
5.	1st tors.	1276	1246	2.4	1241	2.7	1184	7.2
6.	3rd trans.	1282	1249	2.6	1326	3.4	1223	4.6
7.	3rd trans.	1282	1249	2.6	1326	3.4	1223	4.6
			Average:	**2.4**	**Average**:	**1.9**	**Average**:	**4.2**

An additional comparison was conducted using data from the previously referenced study [23], involving a steel-polymer concrete beam modeled with the rigid finite element method. The results are presented in Tab. 7, where δ_R denotes the relative error of the rigid finite element model with respect to the experimental data.

Tab. 7. Comparison of experimental and rigid finite element models-predicted natural frequencies for the 50 × 50 mm, 2 mm wall, 1000 mm long beam

M. no	Mode type	Experiment, Hz	Developed model, Hz	δ, %	Rigid finite element model, Hz	δ_R, %
1.	1st trans.	247	245	0.8	244	1.2
2.	1st trans.	251	245	2.4	245	2.4
3.	2nd trans.	676	657	2.8	664	1.8
4.	2nd trans.	678	657	3.1	665	1.9
5.	1st tors.	1276	1246	2.4	1224	4.1
6.	3rd trans.	1282	1249	2.6	1275	0.5
7.	3rd trans.	1282	1249	2.6	1275	0.5
			Average:	**2.4**	**Average:**	**1.8**

The results indicate that both the developed continuous model and the rigid finite element method provide good agreement with the experimental natural frequencies for the steel-polymer concrete beam. The rigid finite element model demonstrated slightly better overall accuracy, with an average relative error of 1.8 %, compared to 2.4 % for the continuous model. This difference is particularly evident in the higher-order transverse modes (modes 6 and 7), where the rigid model achieved errors as low as 0.5 %, while the continuous model showed consistent deviations of 2.6 %.

For the lower-order transverse modes (modes 1 to 4), both modeling approaches performed similarly, although the rigid finite element model produced slightly smaller errors in most cases. In contrast, the continuous model was more accurate in predicting the

first torsional mode (mode 5), with a relative error of 2.4 %, compared to 4.1 % for the rigid model. This suggests that while the rigid finite element formulation is well suited for capturing bending-dominated behavior, it may be less effective in describing torsional dynamics.

In summary, the rigid finite element model showed marginally higher accuracy in predicting transverse vibration modes, particularly at higher frequencies, while the continuous model provided more consistent results across both bending and torsional modes.

Based on another study [27], a comparison of natural frequencies for a 140 mm × 140 mm beam with a 6 mm wall thickness and 1000 mm length was also conducted. The results, including relative errors δ_{3D} for the three-dimensional finite element model with respect to experimental data, are presented in Tab. 8.

Tab. 8. Comparison of experimental and rigid finite element models-predicted natural frequencies for the 140 × 140 mm, 6 mm wall, 1000 mm long beam

M. no	Mode type	Experiment, Hz	Developed model, Hz	δ, %	Finite element model, Hz	δ_{3D}, %
1.	1st trans.	628	644	2.5	648	3.2
2.	1st trans.	629	644	2.4	648	3
3.	1st tors.	1252	1258	0.5	1265	1
4.	2nd trans.	1526	1561	2.3	1567	2.7
5.	2nd trans.	1527	1561	2.2	1567	2.6
			Average:	**2.0**	**Average:**	**2.5**

The results presented in Tab. 8 show that the developed continuous model predicted natural frequencies with relative errors ranging from 0.5 % to 2.5 %, with an average of 2.0 %. The three-dimensional finite element model showed slightly higher deviations from 1.0 % to 3.2 %, averaging 2.5 %. For the first and second transverse modes (modes 1, 2, 4, and 5), the continuous model exhibited relative errors of approximately 2.2-2.5 %, while the three-dimensional model showed slightly higher discrepancies. The torsional mode (mode 3) was predicted with the highest accuracy by both models, showing the lowest error levels. This suggests that both modeling approaches capture torsional stiffness reliably.

4.4. Discussion

The presented results collectively demonstrate that the developed continuous analytical model offers reliable predictive capability for the dynamic behavior of steel-polymer concrete composite beams across a range of cross-section dimensions and mode types. In all analyzed cases, the model consistently reproduced the experimentally measured natural frequencies with relative errors typically below 3 %, and with a mean error ranging from 0.7 % to 2.4 %, depending on the specific geometry.

The agreement between experimental and predicted receptance functions (Fig. 6) further supports the capability of the continuous model to reproduce not only natural frequencies but also the overall dynamic response of the composite beam. A slight discrepancy in the anti-resonance depth can be observed, which may be attributed to the simplified damping representation adopted in the analytical model.

When compared to high-fidelity three-dimensional finite element models, the continuous model achieved similar or slightly better accuracy in some configurations, particularly for torsional modes and beams with thinner walls. This highlights its ability to efficiently capture global vibrational characteristics without the need for large-scale numerical discretization. While three-dimensional models offer detailed representation of geometry and material interfaces, they do so at significantly higher computational cost. The continuous model, by contrast, provides a valuable trade-off between accuracy and simplicity, particularly in early-stage design, sensitivity studies, or parameter optimization.

Additionally, comparisons with reduced-order modeling approaches such as the rigid finite element method confirmed the robustness of the continuous model. Although the rigid finite element model demonstrated slightly better accuracy in higher-order transverse modes, it also exhibited larger errors in torsional modes. These findings reinforce the observation that the continuous formulation delivers a more balanced representation of bending and torsional behavior – an important feature when dealing with composite beams where both stiffness contributions play a significant role.

The comparative analysis against one-dimensional finite element beam element models based on classical beam theories further underscores the limitations of simplified formulations. The classical approach systematically underestimated torsional and higher-order transverse modes, confirming that such models may not be adequate for vibration analysis of filled sections, particularly when shear deformation and warping effects appear to be significant.

Finally, results obtained for a beam with decreased and increased cross-sectional dimensions (50 × 50 mm, 2 mm wall thickness and 140 × 140 mm, 6 mm wall thickness) confirmed the scalability of the continuous model. Despite substantial differences in cross-section-to-length ratio, the model retained high predictive accuracy.

In summary, the continuous model demonstrated broad applicability, high accuracy, and robustness across different cross-section dimensions. Its performance compared favorably with established finite element methods and reduced-order techniques, supporting its use as an efficient and reliable tool for predicting the dynamic behavior of steel-polymer concrete beams.

5. CONCLUSIONS

This study presented a continuous analytical model for predicting the dynamic behavior of thin-walled steel box beams filled with polymer concrete. The formulation incorporates transverse, torsional, and longitudinal vibrations, enabling the calculation of natural frequencies and mode shapes. Experimental validation demonstrated that the model accurately predicted the first eleven modes, achieving an average relative error below 1.0 % and full agreement in mode shapes.

Comparative analyses with full three-dimensional finite element models, one-dimensional finite element beam models, and rigid finite element formulations confirm the model's competitive accuracy. In particular, the proposed approach matched the fidelity of high-resolution numerical models in bending and torsional modes, while offering reduced computational complexity.

The main limitations of the model stem from the assumption of perfect bonding between the steel shell and polymer concrete core, as well as the reliance on homogenized material properties. These simplifications may affect predictions in cases where interfacial slip, local stress concentrations, or heterogeneous infill properties play a significant role.

Future research will focus on extending the model to account for variable cross-sections, non-uniform, or graded infill materials, and damping characterization to enable complete frequency response prediction. Integration into optimization frameworks

DOI: 10.65731/ama/2026-0029

(benefiting from the significantly lower computational cost compared to detailed 3D FEM models) is also planned to support efficient design of steel-polymer composite structures.

REFERENCES

1. Liu J, Huang S, Li J, Frank Chen Y. Vibration Serviceability of Large-Span Steel–Concrete Composite Beam with Precast Hollow Core Slabs Under Walking Impact. Engineering 2022;19:93–104. https://doi.org/10.1016/j.eng.2021.04.025.
2. Biscontin G, Morassi A, Wendel P. Vibrations of Steel-Concrete Composite Beams. J Vib Control 2000;6:691–714. https://doi.org/10.1177/107754630000600503.
3. Liang J, Yao H, Wang C, Su H. Research on shear behavior of partially encased composite of cellular steel and concrete (PECCS) beam. Structures. 2025;80:109796. https://doi.org/10.1016/j.istruc.2025.109796
4. Hajianmaleki M, Qatu MS. Vibrations of straight and curved composite beams: A review. Compos Struct. 2013;100:218–32. https://doi.org/10.1016/j.compstruct.2013.01.001
5. Euler L. Methodus inveniendi lineas curvas maximi minive proprietate gaudentes. Bousquet Lausanne Geneva; 1744.
6. Timoshenko SP. LXVI. On the correction for shear of the differential equation for transverse vibrations of prismatic bars. Lond Edinb Dublin Philos Mag J Sci 1921;41:744–6. https://doi.org/10.1080/14786442108636264
7. Reddy JN. A Simple Higher-Order Theory for Laminated Composite Plates. J Appl Mech. 1984;51:745–52. https://doi.org/10.1115/1.3167719
8. Rodrigues MAC, Martha LF, Reddy JN, Ruocco E. An Improved Formulation and Analysis of Reddy Beam Model for Framed Structures. Lat Am J Solids Struct. 2024;21. https://doi.org/10.1590/1679-78258103.
9. Berczyński S, Wróblewski T. Vibration of Steel–Concrete Composite Beams Using the Timoshenko Beam Model. J Vib Control 2005;11:829–48. https://doi.org/10.1177/1077546305054678
10. Berczyński S, Wróblewski T. Experimental Verification of Natural Vibration Models of Steel-concrete Composite Beams. J Vib Control 2010;16:2057–81. https://doi.org/10.1177/1077546309350552
11. Dilena M, Morassi A. Vibrations of steel–concrete composite beams with partially degraded connection and applications to damage detection. J Sound Vib. 2009;320:101–24. https://doi.org/10.1016/j.jsv.2008.07.022
12. Cedeño-Rodríguez MD, Yanez SJ, Saavedra-Flores EI, Guzmán CF, Pina JC. Vibration-Based Damage Prediction in Composite Concrete–Steel Structures Using Finite Elements. Buildings. 2025;15. https://doi.org/10.3390/buildings15020200
13. Dunaj P, Dolata M, Berczyński S. Model order reduction adapted to steel beams filled with a composite material. Adv Intell Syst Comput 2019;853:3–13. https://doi.org/10.1007/978-3-319-99996-8_1
14. Wróblewski T, Berczyński S, Abramowicz M. Estimation of the parameters of the discrete model of a steel–concrete composite beam. Arch Civ Mech Eng. 2013;13:209–19. https://doi.org/10.1016/j.acme.2013.01.009
15. Shen J, Pagani A, Arruda MRT, Carrera E. Exact component-wise solutions for 3D free vibration and stress analysis of hybrid steel–concrete composite beams. Thin-Walled Struct. 2022;174:109094. https://doi.org/10.1016/j.tws.2022.109094
16. Carrera E, Giunta G. Refined beam theories based on a unified formulation. Int J Appl Mech. 2010;2:117–43. https://doi.org/10.1142/S1758825110000500
17. Henriques D, Gonçalves R, Sousa C, Camotim D. An efficient assessment of the vibration behaviour of cracked steel–concrete composite beams using GBT. Thin-Walled Struct. 2022;175:109276. https://doi.org/10.1016/j.tws.2022.109276
18. Gonçalves R, Camotim D. Steel-concrete composite bridge analysis using Generalised Beam Theory. Steel Compos Struct. 2010;10:223–43. https://doi.org/10.12989/scs.2010.10.3.223
19. Assem H, Saimi A, Bensaid I, Cheikh A, Dahmane M, Ait Atmane H. Vibration and buckling analysis of quasi-3D porous composite steel-polymer concrete box section beams via DQFEM. Arch Mech Eng. 2025;72:271–92. https://doi.org/10.24425/ame.2025.154737
20. Laouche N, Saimi A, Bensaid I, Dahmane M, Ait Atmane H. A study on the crack presence effect on dynamical behavior of higher-order Quasi-3D composite steel-polymer concrete box section beams via DQFEM. Fract Struct Integr. 2025;19:88–107. https://doi.org/10.3221/IGF-ESIS.73.07
21. Wittbrodt E, Adamiec-Wójcik I, Wojciech S. Dynamics of flexible multibody systems: rigid finite element method. Springer; 2006.
22. Abramowicz M, Berczyński S, Wróblewski T. Modelling and parameter identification of steel–concrete composite beams in 3D rigid finite element method. Arch Civ Mech Eng. 2020;20:103. https://doi.org/10.1007/s43452-020-00100-7
23. Dunaj P, Marchelek K, Berczyński S, Mizrak B. Rigid Finite Element Method in Modeling Composite Steel-Polymer Concrete Machine Tool Frames. Materials. 2020;13. https://doi.org/10.3390/ma13143151
24. Abramowicz M, Pełka-Sawenko A. Comparison of the Finite Element Method and Rigid Finite Element Method During Dynamic Calculations of Steel–Concrete Composite Beams Based on Experimental Results. Materials. 2024;17.https://doi.org/10.3390/ma17246081
25. Okulik T, Dunaj P, Chodźko M, Marchelek K, Powa\lka B. Determination of Dynamic Properties of a Steel Hollow Section Filled with Composite Mineral Casting. In: Gapiński B, Szostak M, Ivanov V editors. Adv. Manuf. II. Cham: Springer International Publishing. 2019; 561–71.
26. Dunaj P, Okulik T, Powa\lka B, Berczyński S, Chodźko M. Experimental Investigations of Steel Welded Machine Tool Bodies Filled with Composite Material. In: Gapiński B, Szostak M, Ivanov V editors. Adv. Manuf. II. Cham: Springer International Publishing. 2019; 61–9.
27. Dunaj P, Berczyński S, Chodźko M, Niesterowicz B. Finite Element Modeling of the Dynamic Properties of Composite Steel–Polymer Concrete Beams. Materials 2020;13.https://doi.org/10.3390/ma13071630
28. Niesterowicz B, Dunaj P, Berczyński S. Timoshenko beam model for vibration analysis of composite steel-polymer concrete box beams. J Theor Appl Mech. 2020;58:799–810. https://doi.org/10.15632/jtam-pl/122389
29. De Silva CW. Vibration: fundamentals and practice. CRC press; 2006.
30. Cowper GR. The Shear Coefficient in Timoshenko's Beam Theory. J Appl Mech. 1966;33:335–40. https://doi.org/10.1115/1.3625046
31. Ertürk A, Özgüven HN, Budak E. Analytical modeling of spindle–tool dynamics on machine tools using Timoshenko beam model and receptance coupling for the prediction of tool point FRF. Int J Mach Tools Manuf. 2006;46:1901–12. https://doi.org/10.1016/j.ijmachtools.2006.01.032
32. Clough RW, Penzien J. Dynamics of Structures. McGraw-Hill; 1975.

This study was funded by the EU grant: "Light construction vertical lathe" POIR.04.01.02-00-0078/16. The research was carried out on a research apparatus purchased as part of project No. RPZP.01.03.00-32-0004/17 and RPZP.01.03.00-32-0001/21. The project was co-financed by the European Union from the European Regional Development Fund under the Regional Operational Program of the West Pomeranian Voivodeship 2014–2020.

Beata Niesterowicz: https://orcid.org/0000-0003-1301-3460

Stefan Berczyński: https://orcid.org/0000-0002-8403-6355

Paweł Dunaj: https://orcid.org/0000-0001-6866-2586